Sensors and Materials, Vol. 30, No. 6 (2018) 1297–1306
MYU Tokyo

S & M 1585

Humidity Sensors Based on High Performance Graphene/Zirconium Dioxide Nanocomposite Material

Wang-De Lin,[1*] Tsan-Chang Chang,[2] and Ren-Jang Wu[3]

[1]Department of Center for General Education, St. Mary's Junior College of Medicine, Nursing and Management, Yilan 26644 Taiwan, ROC
[2]Department of Nursing, Mackay Junior College of Medicine, Nursing, and Management, Taipei 11260 Taiwan, ROC
[3]Department of Applied Chemistry, Providence University, Taichung 43301 Taiwan, ROC

(Received January 29, 2018; accepted April 16, 2018)

Keywords: graphene, ZrO_2, humidity sensor, sensitivity, nanocomposite

This paper reports a novel graphene (G)/zirconium dioxide (ZrO_2) nanocomposite produced using a sol-gel method with various weight percentages of graphene for use in humidity sensors. The morphological and structural properties of the (G/ZrO_2) were characterized using X-ray diffraction (XRD) , Fourier transform infrared (FTIR), transmission electron microscopy (TEM), and energy-dispersive X-ray spectroscopy (EDX). The response characteristics of the sensor, including sensitivity, hysteresis, response time, and recovery time, were investigated from theoretical as well as experimental perspectives. Experimental results revealed a linear functional relationship between shifts in the impedance of the sensor and variations in relative humidity. The sensor with 40 wt% G/ZrO_2 nanocomposite demonstrated a sensitivity (S = 4011) exceeding that of the other samples. At all humidity levels, the humidity hysteresis values remained low, and the response and recovery times were very rapid (5 and 20 s, respectively). These results demonstrate the considerable potential of using G/ZrO_2 nanocomposites in the further development of humidity sensors.

1. Introduction

The monitoring of humidity levels is crucial to the operation of medical equipment as well as numerous food production and industrial systems.[1,2] Several ceramic materials, including TiO_2,[3] ZnO,[4] SnO_2,[5] B_2O_3,[6] and ZrO_2,[7] have proven particularly effective, due to their superior mechanical, chemical, and thermal stability.[8] A variety of techniques and devices are used for the measurement of humidity, including impedance,[9] capacitance,[10] optics,[11] resistance,[12] and the quartz crystal microbalance.[13] Regardless of the structure, all such devices must be relatively small, easy to fabricate, and inexpensive, while providing high sensitivity, low humidity hysteresis, and rapid response and recovery times.[14]

Depending on temperature, ZrO_2 can be found in the three phases: monoclinic, tetragonal,

*Corresponding author: e-mail: newwander@smc.edu.tw
http://dx.doi.org/10.18494/SAM.2018.1916

ISSN 0914-4935

and cubic. Below 1150 ℃, this ceramic material has a monoclinic structure with high degree of thermal and chemical stability and excellent toughness.[15] This has led numerous researchers to investigate the application of ZrO_2 materials in humidity sensors.[7,16–18] Unfortunately, the sensing performance of ZrO_2 is inhibited by pronounced hysteresis.[7] Graphene has a large specific surface area, a large number of reactive sites, high electrical mobility, and excellent thermal conductivity, leading to its widespread use in humidity sensing applications.[19] Recent studies have favoured the use of methylene blue (MB) and rhodamine B dyes (RB) were degraded from water using ZrO_2 and zirconium oxide/graphene composites (ZrO_2/GR) as photocatalyst.[20] However, no previous study has reported on the use of G/ZrO_2 nanocomposite material for use in humidity sensors.

Is this study, we developed a novel humidity sensor based on a G/ZrO_2 nanocomposite. The humidity-sensing properties of the sensor were measured over a wide range of relative humidity (RH) values (12–90%) at room temperature. Results from repeated experiments confirm that the proposed sensor has excellent linearity, sensitivity (S = 4011), negligible hysteresis (<2.0%), quick response time (5 s), and rapid recovery time (20 s).

2. Materials and Methods

2.1 Materials

Zirconium oxychloride ($ZrClO_2 \cdot 8H_2O$), anhydrous alcohol (C_2H_5OH), and polyvinyl alcohol (PVA) were purchased from Sigma-Aldrich Co., Inc. (USA). High-purity graphene (G) films (>99%) were supplied by Sigma-Aldrich Co., Inc. (USA). Water was distilled and deionized (DI) using a Milli-Q water purification system (Millipore Corp. France).

2.2 Fabrication of G/ZrO_2 nanocomposites

G/ZrO_2 nanocomposite materials were produced by mixing a specific weighed ratio of graphene and ZrO_2. We began by mixing 3.22 g zirconium oxychloride ($ZrClO_2 \cdot 8H_2O$) with 50 ml anhydrous alcohol under magnetic stirring for 30 min while heating the solution to 30 ℃.[3] The second step entailed the preparation of graphene powder at specific concentrations. The graphene samples were added to the ZrO_2 solution and held at 30 ℃ for 3 d until a powder had formed. The samples were then calcined in air at 600 ℃ for 2 h. Various ratios of the sensing material (5, 10, 20, 30, 40, and 50 wt%) were tested.

2.3 Characterization of G/ZrO_2 nanocomposites

The crystal structure of the G/ZrO_2 nanocomposites was characterized using a XRD-6000 Shimadzu X-ray diffractometer with Cu Kα radiation (λ = 0.15405 nm) and a 2θ range of 10–80°. We also employed a Fourier transform infrared spectrometer (FT-IR D8 Series, Canada) equipped with a mercury–cadmium–telluride (MCT) detector. Spectra of NaCl crystals with dimensions of 25 × 4 mm^2 (Spectral Systems Inc., #955-3616; USA) were collected

in transmission mode at room temperature under atmospheric pressure using a mean of 64 scans from 400 to 5000 cm^{-1} at a resolution of 2 cm^{-1}. The morphology and structure of the G/ZrO_2 nanocomposites were investigated using transmission electron microscopy and energy dispersive X-ray spectroscopy (TEM/EDX, JEOL JEM-2010), during which the samples were supported on carbon-coated copper grids.

2.4 Fabrication of humidity sensor

Sensor chips were fabricated by dip coating the alumina substrate (10 × 5 mm^2) to form a pair of comb-like gold electrodes, followed by the application of PVA as a binder using spin coating at a rotation speed of 1000 rpm. The resulting sensing chips were then heated to 70 ℃ and held at that temperature for 1 h before undergoing calcination at 600 ℃ for 2 h.

2.5 Sensing system

Figure 1 presents a schematic diagram showing the humidity response measurements obtained from the proposed device using a dynamic flow system with sensors housed within a glass chamber. Dynamic testing was conducted by cycling the relative humidity between 12% and 90% by adjusting the air/water ratio. In this experiment, the RH was measured using a hygrometer (Rotronic) with an accuracy of ±0.1% RH. The impedance response of the sensing film with respect to the humidity was measured by using a chemical impedance analyzer (Delta United, DU 6010) with an applied AC voltage of 1 V and frequency of 1 kHz.

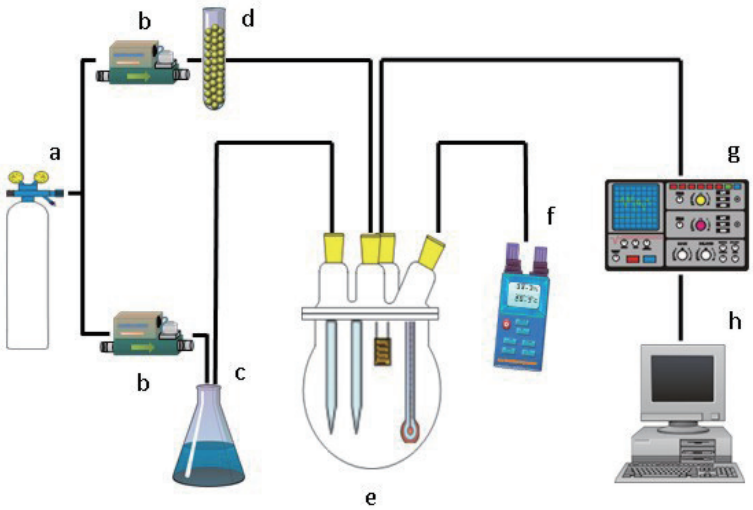

Fig. 1. (Color online) Schematic diagram of experimental setup: (a) air, (b) gas flow controller, (c) water, (d) molecular sieve and desiccating agent, (e) detecting chamber and thermostat, (f) humidity hygrometer, (g) L.C.R.Z. meter, and (h) PC.

3. Results and Discussion

3.1 Structure characterization

Figure 2 shows the XRD spectra of graphene, ZrO_2, and G/ZrO_2 (at 5, 10, 20, 30, 40, and 50 wt%). As shown in spectrum 2(a), the graphene yielded a (002) diffraction peak at 26.42°.[19] spectrum 2(b) shows peaks at 28.06, 30.08, 35.08, 50.06, and 60.19° (2-θ degree), which can be attributed to the monoclinic phase (JCPDS-07-0343) of the ZrO_2 structure.[21] spectrum 2(c-h) are the spectra of the various G/ZrO_2 samples, revealing no other crystalline phases. These results indicate that the sensing material was a simple mixture.

Figure 3 shows the FTIR spectra of graphene, ZrO_2, and various G/ZrO_2 nanocomposite samples. As shown in spectrum 3(a), graphene has a band at 2323 cm^{-1} associated with the C=O stretching mode,[22] which may be due to the environmental adsorption of CO_2 on the surface of the graphene. The FTIR spectrum of ZrO_2, 3(b), has bands at 501 and 688 cm^{-1}, corresponding to the stretching vibrations of Zr–O. The broad, weak bands at 3357 and 1589 cm^{-1} can be attributed to the stretching vibration of hydroxyl groups and interlayer water molecules.[23] The FTIR spectra of the G/ZrO_2 nanocomposite samples are similar to 3(c)–(h), with the main bands corresponding to graphene and ZrO_2. These results demonstrate that the ZrO_2 effectively covered the surface of the graphene.

The morphology of ZrO_2, graphene, and 40 wt% G/ZrO_2 nanocomposite were characterized by TEM, as shown in Fig. 4. Figure 4(a) shows that the morphology of ZrO_2 is primarily spheres with a diameter of approximately 30–40 nm. Figure 4(b) shows smooth graphene sheets stacked irregularly on the surface of the nanocomposite. Figure 4(c) is a TEM image

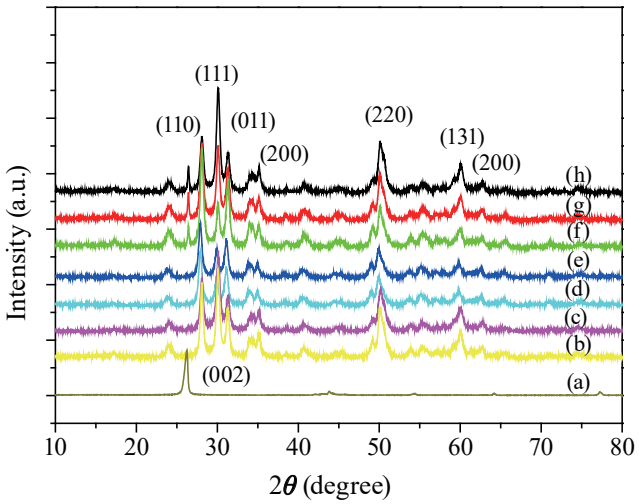

Fig. 2. (Color online) XRD patterns of (a) G, (b) ZrO_2, (c) 5 wt% G/ZrO_2, (d) 10 wt% G/ZrO_2, (e) 20 wt% G/ZrO_2, (f) 30 wt% G/ZrO_2, (g) 40 wt% G/ZrO_2, and (h) 50 wt% G/ZrO_2.

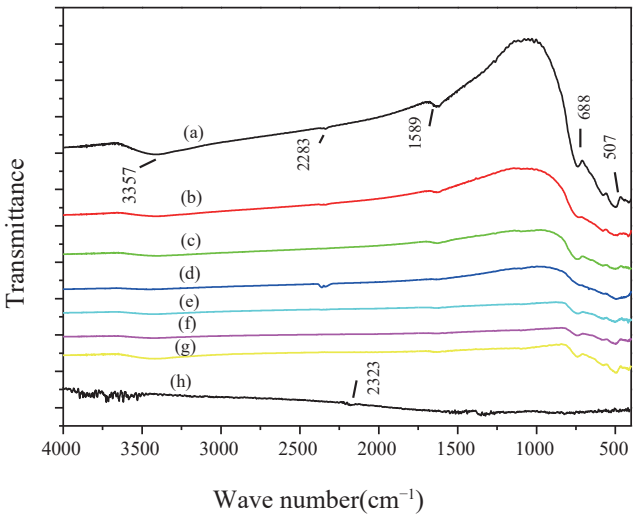

Fig. 3. (Color online) FT-IR spectra of (a) ZrO_2, (b) 5 wt% G/ZrO_2, (c) 10 wt% G/ZrO_2, (d) 20 wt% G/ZrO_2, (e) 30 wt% G/ZrO_2, (f) 40 wt% G/ZrO_2, (g) 50 wt% G/ZrO_2, and (h) G.

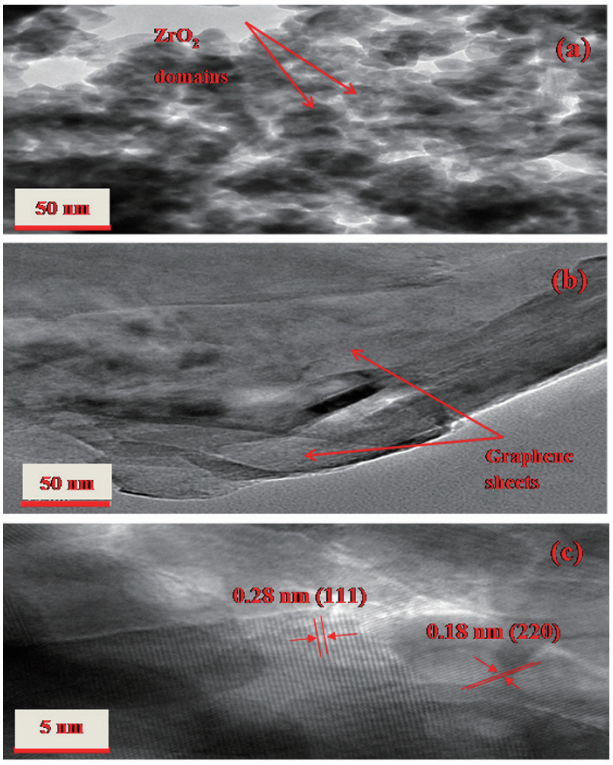

Fig. 4. (Color online) TEM images of (a) ZrO_2, (b) graphene, and (c) 40 wt% G/

revealing lattice fringes on the 40 wt% G/ZrO_2 nanocomposite. The *d*-spacing of fringe spacing (*d*) at 0.18 and 0.28 nm can be attributed to the (220) plane of tetragonal and (111) plane of monoclinic ZrO_2, respectively.[24] As shown in Fig. 5, the EDX spectrum of the 40 wt% G/ZrO_2 nanocomposites reveals peaks of Zr, C, and O. This provides further proof that the sensing material is a simple mixture.

3.2 Humidity sensing properties

Figure 6 illustrates the dependence of impedance on RH for different content of G/ZrO_2 nanocomposite. At low RH, the impedance decreased gradually with an increase in RH; however, at high RH, the impedance decreased dramatically. Over an RH range of 12% to 90%, pure ZrO_2 and hydrophobic property of graphene exhibited poor response characteristics, particularly at low humidity levels. In contrast, we observed a steep drop off in the impedance of the hybrid samples over the entire RH% range, thereby demonstrating the contribution of graphene to enhancing humidity sensing performance. Increasing the proportion of graphene from 5 to 50 wt% in G/ZrO_2 led to a corresponding increase in sensitivity. This could be attributed to blockage of the transmission of charge carriers across the surface of the ZrO_2. Increasing RH from 12% to 90% decreased the impedance of the 40 wt% G/ZrO_2 nanocomposite from 14200 to 3.54 kΩ; i.e., variations of approximately four orders of

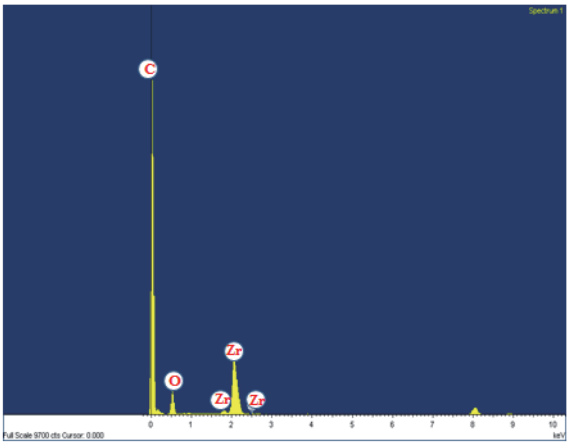

Fig. 5. (Color online) EDX spectrum of the 40 wt% G/ZrO_2 nanocomposites.

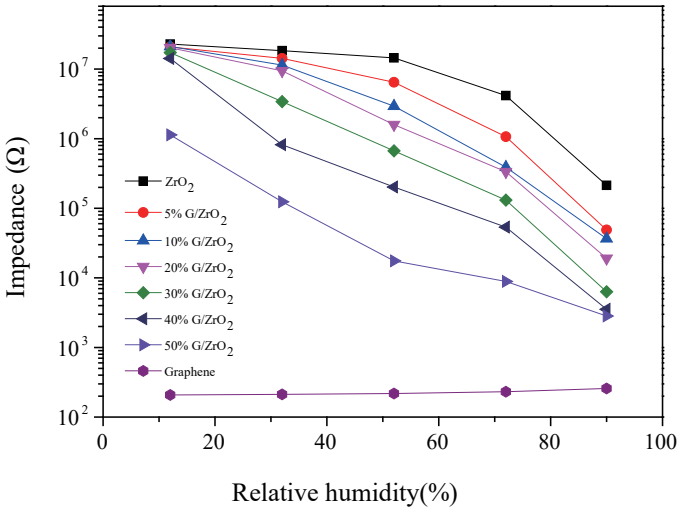

Fig. 6. (Color online) The dependence of impedance on RH for different content of G/ZrO_2 nanocomposite.

magnitude. The RH sensitivity (S) of the humidity sensor can be defined as $S = R_d/R_h$, where R_d is the resistance of the sensor under dry conditions (12% RH), and R_h is the resistance at a specific humidity level.[25] Figure 7 and Table 1 present the S values when RH was varied between 12% and 90%, as follows: 5 wt% (425.9), 10 wt% (578.5), 20% (1058), 30 wt% (2730), 40wt% (4011), and 50wt% (400.7). The 40 wt% G/ZrO_2 nanocomposite exhibited the highest responsiveness to humidity (S = 4011); therefore, we selected this nanocomposite for further analysis of RH sensing characteristics.

Humidity hysteresis was investigated by increasing the humidity from 12 to 90% to promote the adsorption of water molecules and then decreasing it to 12% to promote desorption. Humidity hysteresis error (H) was calculated using the following expression: $H = \Delta f_{max}/f_{fs} \times 100\%$, where Δf_{max} is the maximum hysteresis error and f_{fs} is the full-scale response output. Table 2 presents the hysteresis values from RH of 12 to 72%. The adsorption and desorption curves obtained from this sensor nearly coincide. We determined that the humidity hysteresis error of the 40 wt% G/ZrO_2 nanocomposite was less than 1.95%, which represents performance on par with the best humidity sensors reported in the literature.[18,26]

Response and recovery times are important characteristics in estimating the performance of a humidity sensor. These values are defined as the time required for the total impedance of a sensor to change by 90%.[27] As shown in Fig. 8, the sensor response time of the 40 wt% G/ZrO_2 device (humidification from 12 to 90% RH) was only 5 s, and the recovery time (desiccation from 90 to 12% RH) was approximately 20 s. This clearly demonstrates the potential of using 40 wt% G/ZrO_2 in the detection of relative humidity. The humidity sensing properties of the present humidity sensor were compared with those of sensors in the literature[19,28–32] in Table 3. It can be found that our sensor exhibits outstanding sensing properties with high sensitivity, rapid response/recovery times, and small hysteresis in the

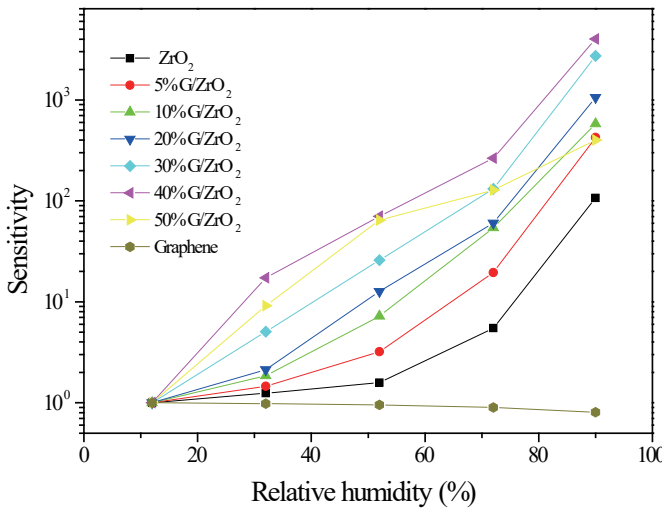

Fig. 7. (Color online) Variation of sensitivity with humidity for different content of G/ZrO_2 nanocomposite.

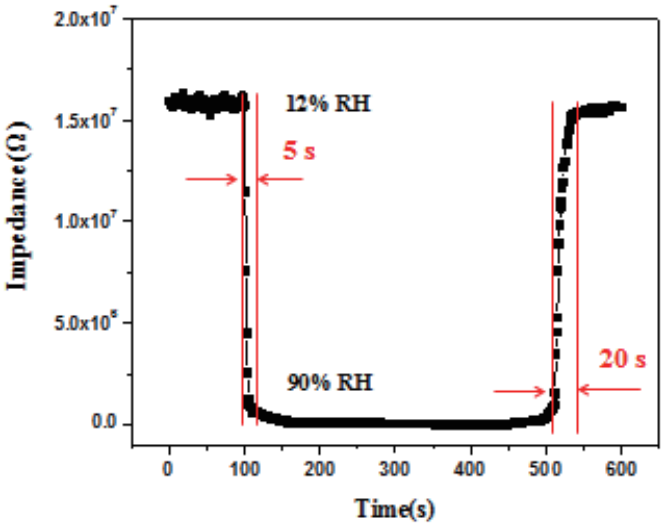

Fig. 8. (Color online) Response and recovery characteristics of 40 wt% G/ZrO_2 nanocomposite.

Table 1
Calculated sensitivity values for different content of G/ZrO_2 nanocomposite.

Sample	ZrO_2	5% ZrO_2	10% ZrO_2	20% ZrO_2	30% ZrO_2	40% ZrO_2	50% ZrO_2	Graphene
12%	1	1	1	1	1	1	1	1
32%	1.25	1.46	1.85	2.14	5.06	17.3	9.15	0.98
52%	1.58	3.21	7.20	12.7	25.8	70.3	64.6	0.95
72%	5.50	19.5	54.3	60.3	131.6	265.3	127.8	0.90
90%	107.1	425.9	578.5	1058	2730	4011	400.7	0.80

Table 2
Calculated hysteresis values for 40% G/ZrO_2 nanocomposite.

RH	12%	32%	52%	72%
Hysteresis	0.03%	1.95%	0.95%	0.78%

Table 3
Humidity sensor performance of this work compared with the literatures.

Sensing material	Fabrication method	Measurement range	Response/ recovery time (s)	References
Graphene/TiO_2	Sol–gel method	12–90% RH	128/68	[19]
RGO/SnO_2	Hydrothermal synthesis	11–97% RH	102/100	[28]
GO/ZnO	Sol–gel immersion	11.3–97.3% RH	9/5	[29]
GO/SnO_2/PANI	*In-situ* oxidative polymerization	0–97% RH	7/2	[30]
Graphene/ZnO	Sol–gel method	12–90% RH	5/90	[31]
RGO/MoS_2	Hydrothermal	10–90% RH	30/253	[32]
Graphene/ZrO_2	Sol–gel method	12–90% RH	5/20	This paper

detection of humidity.

To evaluate the stability of the G/ZrO_2 nanocomposite fabricated sensor at two different temperatures of 25 and 35 °C, we have exposed the sample in the air for 144 h followed by a measurement of the impedance to various RH levels. Figure 9 shows in the curves, the product exhibited excellent stability, and there was no significant change in the impedance during this period. We can see from the picture that as the temperature increases, the impedance of the sensor decreases, the reason would be that increasing temperature induces more H_3O^+ and H_2O to hydrate into H^+. The increasing concentration of H^+ improves the conductivity of the sensing materials. The conduction increases, and then the impedance of the sensor decreases.[26]

3.3. Humidity sensing mechanism

The G/ZrO_2 nanocomposites exhibited humidity-sensing properties superior to those of pure graphene and ZrO_2. This may be due to the structural and morphological characteristics as well as the hydrophilic functional groups (e.g., hydroxyl groups) attached on the surface. The accumulation of ZrO_2 nanoparticles increases the likelihood that water molecules could be obstructed from the inner sensing material. This may explain the hysteresis under high humidity shown in Fig. 10(a). In contrast, the G/ZrO_2 nanocomposites provide numerous channels by which water molecules could penetrate the surface and thereby come into contact with the inner sensing materials, as shown in Fig. 10(b). Under low humidity, the probability of contact between water molecules and G/ZrO_2 nanocomposite material is low. This means that only the outer particles came into contact with water molecules. The fact that the water molecules do not form a continuous layer makes it difficult for the transfer of H_2O or H_3O^+ across the discontinuous water layer. This explains why the G/ZrO_2 nanocomposite exhibit

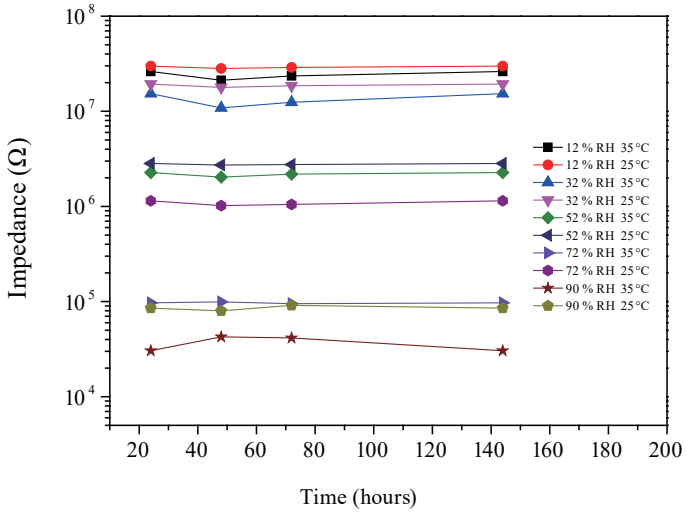

Fig. 9. (Color online) Stability of the humidity sensor based on G/ZrO_2 nanocomposite at temperatures of 25 and 35 °C.

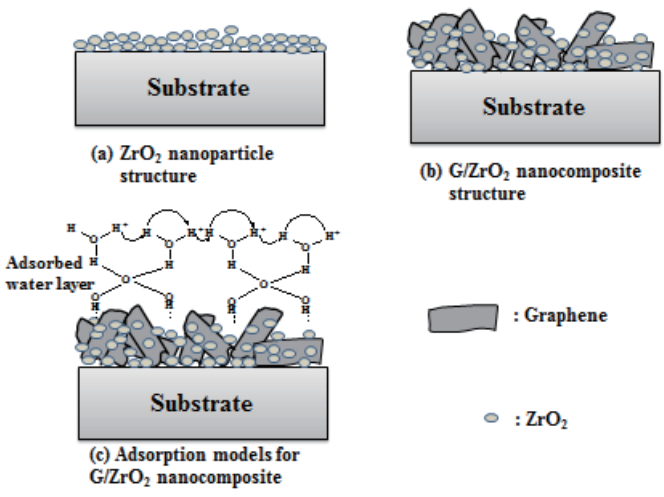

Fig. 10. (Color online) An illustration of the humidity sensing mechanism of (a) ZrO_2 nanoparticle structure, (b) G/ZrO_2 nanocomposite structure, and (c) adsorption models for G/ZrO_2 nanocomposite structure.

higher impedance at lower humidity levels. As shown in Fig. 10(c), increasing the relative humidity resulted in the formation of one or more serial water layers among the particles of the G/ZrO_2 nanocomposite. The serial water layers accelerate the transfer of H_2O or H_3O^+. Ernsberger and Casalbore-Miceli *et al*. outlined an ion transfer mechanism involving the transfer of H_2O or H_3O^+ on serial water layers, as follows: $H_2O + H_3O^+ \rightarrow H_3O^+ + H_2O$.[33,34] This makes the G/ZrO_2 nanocomposites more sensitive to humidity, which is manifest as high sensitivity, low humidity hysteresis, and quick response and recovery times, probably due to the irregular stacking of smooth graphene sheets.

4. Conclusions

In this study, we succeeded in the fabrication of G/ZrO_2 nanocomposites with a high degree of sensitivity to humidity, far exceeding the performance of G/ZrO_2. A sensor made with 40 wt% graphene nanocomposite provided the highest sensitivity (S = 4011) with low humidity hysteresis (less than 2.0%), excellent linearity, and variations in impedance exceeding four orders in magnitude over an RH range of 12–90% at room temperature. The 40 wt% G/ZrO_2 nanocomposite demonstrated a quick response time of 5 s and a recovery time and 20 s.

Acknowledgments

The authors thank the Ministry of Science and Technology (grant no. MOST 103-2113-M-562-001-) of Taiwan for support and gratefully acknowledge Department of Applied Chemistry in Providence University for their beneficial help in fabricating humidity sensors.

References

1 E. Traversa: Sens. Actuators, B **23** (1995) 135.
2 T. A. Blank, L. P. Eksperiandova, and K. N. Belikov: Sens. Actuators, B **228** (2016) 416.
3 K. P. Biju and M. K. Jain: Sens. Actuators, B **128** (2008) 407.
4 L. Gu, K. Zheng, Y. Zhou, J. Li, X. Mo, G. R. Patzke, and G. Chen: Sens. Actuators, B **159** (2011) 1.
5 V. K. Tomer and S. Duhan: Sens. Actuators, B **223** (2016) 750.
6 E. Şentürk, S. Duman, S. Bağcı, H. S. Soykan, and Z. Aslanoğlu: Sens. Actuators, A **240** (2016) 80.
7 J. Wang, M. Y. Su, J. Q. Qi, and L. Q. Chang: Sens. Actuators, B **139** (2009) 418.
8 L. Almar, A. Tarancón, T. Andreu, M. Torrell, Y. Hu, G. Dezanneau, and A. Morata: Sens. Actuators, B **216** (2015) 41.
9 M. J. Zouaoui, B. Nait-Ali, N. Glandut, and D. S. Smith: J. Eur. Ceram. Soc. **36** (2016) 163
10 W. C. Wang, Y. T. Tian, K. Li, E. Y. Lu, D. S. Gong, and X. J. Li: Appl. Surf. Sci. **273** (2013) 372.
11 P. J. Thomas and J. O. Hellevang: Sens. Actuators, B **247** (2017) 284.
12 A. Sun, L. Huang, and Y. Li: Sens. Actuators, B **139** (2009) 543.
13 Y. Yao and Y. Xue: Sens. Actuators, B **211** (2015) 52.
14 A. S. Garde: J. Alloys Compd. **617** (2014) 367.
15 H. C. Madhusudhana, S. N. Shobhadevi, B. M. Nagabhushana, B. V. Chaluvaraju, M. V. Murugendrappa, R. Hari Krishna, H. Nagabhushana, and N. R. Radeep: J. Asian Ceram. Soc. **4** (2016) 309.
16 M. K. Jain, M. C. Bhatnagar, and G. L. Sharma: Sens. Actuators, B **55** (1999) 180.
17 M. Su and J. Wang: Sens. Lett. **9** (2011) 670.
18 Z. Wang, Y. Lu, S. Yuan, L. Shi, Y. Zhao, M. Zhang, and W. Deng: J. Colloid Interf. Sci. **396** (2013) 9.
19 W. D. Lin, C. T. Liao, T. C. Chang, S. H. Chen, and R. J. Wu: Sens. Actuators, B **209** (2015) 555.
20 S. Rani, M. Aggarwal, M. Kumar, S. Sharma, and D. Kumar: Water Sci. **30** (2016) 55.

21 L. Renuka, K. S. Anantharaju, S. C. Sharma, H. Nagabhushana, Y. S. Vidya, H. P. Nagaswarupa, and S. C. Prashantha: J. Alloys Compd. **695** (2017) 382.
22 J. T. Illakkiya, P. U. Rajalakshmi, and R. Oommen: Surf. Coat. Technol. **307** (2016) 65.
23 S. Zinatloo-Ajabshir, M. Salavati-Niasari: J. Mol-Liq. **216** (2016) 545.
24 R. K. Singha, A. Shukla, A. Yadav, S. Adak, Z. Iqbal, N. Siddiqui, and R. Bal: Appl. Energy **178** (2016) 110.
25 W. D. Lin, D. S. Lai, M. H. Chen, R. J. Wu, and F. C. Chen: Mater. Res. Bull. **48** (2013) 3822.
26 M. Su, J. Wang, H. Du, P. Yao, Y. Zheng, and X. Li: Sens. Actuators, B **161** (2012) 1038.
27 T. Alizadeh and M. Shokri: Sens. Actuators, B **222** (2016) 728.
28 D. Zhang, H. Chang, P. Li, R. Liu, and Q. Xue: Sens. Actuators, B **225** (2016) 233.
29 Z. Yuan, H. Tai, X. Bao, C. Liu, Z. Ye, and Y. Jiang: Mater. Lett. **174** (2016) 28.
30 D. Zhang, D. Wang, X. Zong, G. Dong, and Y. Zhang: Sens. Actuators, B **262** (2018) 531.
31 Z. Zhu, Y. T. Guo, T. C. Chang, R. J. Wu, and W. D. Lin: Nanosci. Nanotechnol. Lett. **10** (2018) 46.
32 S. Y. Park, J. E. Lee, Y. H. Kim, J. J. Kim, Y. S. Shim, S. Y. Kim, M. H. Lee, and H. W. Jang: Sens. Actuators B **258** (2018) 775.
33 F. M. Ernsberger: J. Am. Ceram. Soc. **66** (1983) 747.
34 G. Casalbore-Miceli, M. J. Yang, N. Camaioni, C. M. Mari, Y. Li, H. Sun, and M. Ling: Solid State Ionics **131** (2000) 311.